Quantitative assessment of the effects of microstructure on the stability of retained austenite in TRIP steels

S. Zhang *, K.O. Findley

Department of Metallurgical and Materials Engineering, Colorado School of Mines, Golden, CO 80401, USA

Abstract

The stability of retained austenite (RA) in transformation-induced plasticity steels (TRIP) is affected by many factors, including chemical composition, RA grain size, neighboring microconstituents of RA and temperature. The composition and microstructure factors are interrelated, so it is difficult to separate out the influence of each individually. In this investigation, methods were developed to study the effects of RA grain size and neighboring microconstituents in a silicon-alloyed low-carbon (0.2C–1.6Si–1.6Mn) TRIP steel. Uniaxial tensile tests, performed at $-20\,°C$, room temperature ($20\,°C$) and $40\,°C$, were interrupted at several strain levels. Scanning electron micrographs were obtained from each condition, and RA was quantified using a novel technique called the categorical chord-length distribution (CCLD), which enables microstructural quantification based on specific neighboring microconstituents. The results show that RA adjacent to bainitic ferrite (BF) and fine RA grain size are correlated with higher RA stability. A modified Burke–Matsumura–Tsuchida stability model was developed to kinetically analyze the effects of microstructure on RA transformation. The CCLD and kinetic modeling analysis indicates that the stability of RA inside BF is less sensitive to the testing temperature than RA inside polygonal ferrite (PF), and thermodynamic analysis of the driving force for transformation as a function of temperature and carbon content implies that there is a higher carbon content in RA inside BF. Additionally, nanohardness tests showed that the hardnesses of BF and PF are not significantly different after moderate amounts of deformation. Thus, the enhanced stability of RA inside BF compared to PF is more strongly related to the elevated carbon content of RA inside BF rather than stress partitioning differences for RA adjacent to BF or PF.
© 2012 Acta Materialia Inc. Published by Elsevier Ltd. All rights reserved.

Keywords: TRIP steel; Retained austenite; Microstructure

1. Introduction

Retained austenite (RA) has a critical role in the superior mechanical properties of certain advanced high-strength steels due to the transformation-induced plasticity (TRIP) effect. Strain-induced transformation from RA to martensite increases the work hardening rate of TRIP steel, which delays the onset of necking and therefore increases the ductility. The most common versions of multiphase TRIP steels have microstructures composed of ferrite, bainite, RA and martensite. Typically, TRIP steels are cold-rolled to their final dimension, intercritically annealed, austempered and then cooled to room temperature. During austempering, intercritical austenite is decomposed into bainite, and excess carbon is partitioned to austenite. The elevated carbon content in austenite lowers its martensitic start temperature to below room temperature, thus a significant volume fraction of RA and a small amount of martensite is present in the room-temperature microstructure. The bainite formed during austempering is usually carbide free due to the high silicon content of TRIP steels and is sometimes referred to as "bainitic ferrite" (BF); ferrite formed during intercritical annealing is correspondingly referred to as "polygonal ferrite" (PF) to avoid ambiguity.

* Corresponding author. Address: 1500 Illinois St., Hill Hall, Golden, CO 80401, USA. Tel.: +1 303 596 1817; fax: +1 303 273 3016.
  E-mail address: szhang@mines.edu (S. Zhang).

The stability of RA is crucial to the mechanical properties of the steel. It is desirable to produce RA with proper stability so that strain-induced martensitic transformation (SIMT) occurs gradually with increasing plastic strain. RA with low stability transforms at small strains and does not improve the ductility of the steel. The stability of RA is affected by the chemical composition of RA [1], the size/morphology of RA [2,3] and the neighboring microconstituents [3,4].

The effects of chemical composition, specifically carbon and manganese content, and temperature can be described by the chemical driving force for martensitic transformation through an equation such as the following [5]:

$$\Delta G^{ch} = -7381.6 + 69447X_C + 19296X_{Mn}$$
$$- 38776X_CX_{Mn} + (6.7821 - 33.45X_C)T \quad (1)$$

where ΔG^{ch} is the chemical driving force of martensitic transformation, X_c is the mole fraction of carbon, X_{Mn} is the mole fraction of manganese and T is the temperature in kelvin. Eq. (1) shows that both carbon and manganese are potent stabilizers of RA. The stability of RA also increases with increasing temperature; the temperature dependence can be derived by differentiating ΔG^{ch} by temperature in Eq. (1):

$$\frac{\partial \Delta G^{ch}}{\partial T} = 6.7821 - 33.45X_c \quad (2)$$

Eq. (2) shows that a positive change in temperature results in a positive change in ΔG^{ch}; thus, the transformation driving force decreases and RA is more stable. Tensile tests conducted over a range of temperatures on TRIP steels exhibit the expected variation of RA stability with temperature [6–9].

The stability of RA is also affected by its size [2,3], where fine RA grain size is found to increase its stability. The effects of RA grain size can be attributed to the probability of martensitic nucleation and the energy barrier to the growth of martensite. Fine RA grains have fewer pre-existing martensite nuclei and therefore a lower probability of transformation. The interfacial energy of the emerging martensite–RA interface also acts as an energy barrier; in smaller RA grains, the molar interfacial energy is larger than that in larger RA grains.

Finally, neighboring microconstituents, especially BF, may affect the stability of RA. Timokhina et al. [3] showed that RA surrounded by BF is more stable than RA inside PF. Grajcar [10] speculated that RA adjacent to BF has a higher carbon content due to shorter diffusion paths and is stabilized thermodynamically, as shown in Eq. (1). It is also possible that BF stabilizes RA via stress partitioning. Compared to PF, the harder BF [11] might shield neighboring RA from externally applied stress. The stress partitioning mechanism is based on the theoretical calculation that a hard microconstituent adjacent to RA will reduce the hydrostatic pressure without changing the equivalent stress [12]. Reducing the hydrostatic pressure in turn reduces the mechanical driving force for transformation [1]:

$$\frac{\partial \Delta g^{\sigma}}{\partial \bar{\sigma}} = -0.715 - 0.3206 \frac{\sigma_h}{\bar{\sigma}} \quad (3)$$

where σ_h is the hydrostatic pressure and $\bar{\sigma}$ is the equivalent stress. It is also noteworthy that RA inside BF has a significantly different size and morphology from RA inside PF, which may also affect how stress is partitioned between the microconstituents.

As shown in the above discussion, many factors influence RA stability. However, it is difficult to separate the contribution of each factor, particularly near BF, where the chemical driving force, RA grain size and surrounding microconstituents may all promote stability compared to RA near PF. The objective of the present investigation is to quantitatively monitor RA stability as a function of neighboring microconstituents and employ a kinetics analysis to separate out the influences of the chemical driving force, the RA grain size and the surrounding microconstituents.

2. Experiments

The material used in this study is a silicon-alloyed low-carbon TRIP steel, the composition of which is given in Table 1. The steel is cold rolled to a thickness of 1.2 mm, intercritically annealed at 790 °C, austempered at 375 °C for 500 s and water cooled to room temperature.

The steel was deformed in interrupted tensile tests at controlled temperatures. Steel sheets 1.2 mm thick were machined according to the ASTM E-8 standard and deformed to different levels of tensile strain with screw-driven tensile testing frames. The tests were performed at a displacement rate of 0.0423 mm s^{-1}. For each heat treatment condition, one of the tests was pulled to failure and the other tests were stopped at specified strains. Tensile tests were performed at −20 °C, room temperature (20 °C) and 40 °C. Specimens were submerged in an ethanol bath cooled by liquid nitrogen to maintain the tensile test temperature at −20 °C. Specimens were submerged in an oil bath for the 40 °C tensile tests. Each sample was immersed for 5 min to allow the temperature to equilibrate before tensile testing.

After the tensile tests, samples were taken from gauge sections of the tensile strips for metallography. In fractured specimens, samples were taken from the gauge section away from the region of necking. Non-deformed samples were taken from grip sections of the tensile strips. Each specimen was tempered at 200 °C for 2 h so that martensite could be differentiated from RA [3,13]. The specimens were then ground and polished using standard metallography procedures before being etched in 4% picric acid in ethanol solution. A JEOL field emission scanning electron microscope (FE-SEM) was used to characterize the microstructures. Five to seven images of each specimen were taken at 6000× magnification.

Table 1
Chemical composition of the steel (in wt.%).

C	Mn	Si	Ni	Cr	Mo	Ti	Nb	V	Al	N	S	P	Cu
0.19	1.59	1.63	0.02	0.03	<0.01	0.003	<0.003	<0.003	0.036	0.019	0.002	0.013	0.01

3. Quantitative metallography

Quantitative microstructure characterization was performed on the SEM images of the microstructures. Fig. 1 shows SEM micrographs of nondeformed and deformed microstructures at various testing temperatures. An advanced characterization technique called categorical chord-length distribution (CCLD) was developed and utilized to determine the volume fraction, size distribution and adjacent microconstituents of RA in the heat-treated steels at each strain level [14].

The concept of CCLD is an extension of the chord-length distribution (CLD) [15]. In addition to the length of a chord, each chord is categorized by the type of interface where the ends of chords lie (Fig. 2). When RA is the phase of interest, there are three types of interfaces in TRIP steel: RA–BF, RA–PF and RA–martensite. To determine the CCLD, an array of test probes (grid) is superimposed on the micrograph, and chords are the segments of the test probes that lie within RA. The length of each chord is measured and the chord is categorized according to the interfaces where each end falls. The CCLD is therefore designated by $n^{ij}(l)$, which is the distribution density function of chords of length l and category ij, where i and j are the types of interfaces where the ends of the chords lie. There are six possible categories of RA based on combinations of interfaces. Super-categories of physical relevance can be defined by combining two or more categories. For example, "Adjacent to PF" can be defined by combining all categories that have at least one chord-end lying on a RA–PF interface. The current study focuses on four (super-) categories, which are defined in Table 2.

The average grain size and volume fraction of RA can be derived from the CCLD. The average constituent size can be calculated by the average of the CCLD:

$$\langle D^{ij} \rangle = \int_0^\infty n^{ij}(l) l \, dl \qquad (4)$$

where $\langle D^i \rangle$ is the average size of the RA of category ij. The volume fraction of RA can be calculated by:

$$V_v^{ij} = \frac{\langle D^{ij} \rangle N^{ij}}{L} \qquad (5)$$

where V_v^{ij} is the volume fraction of RA of category ij and N^{ij} is the total number of chords measured with probes of total length of L.
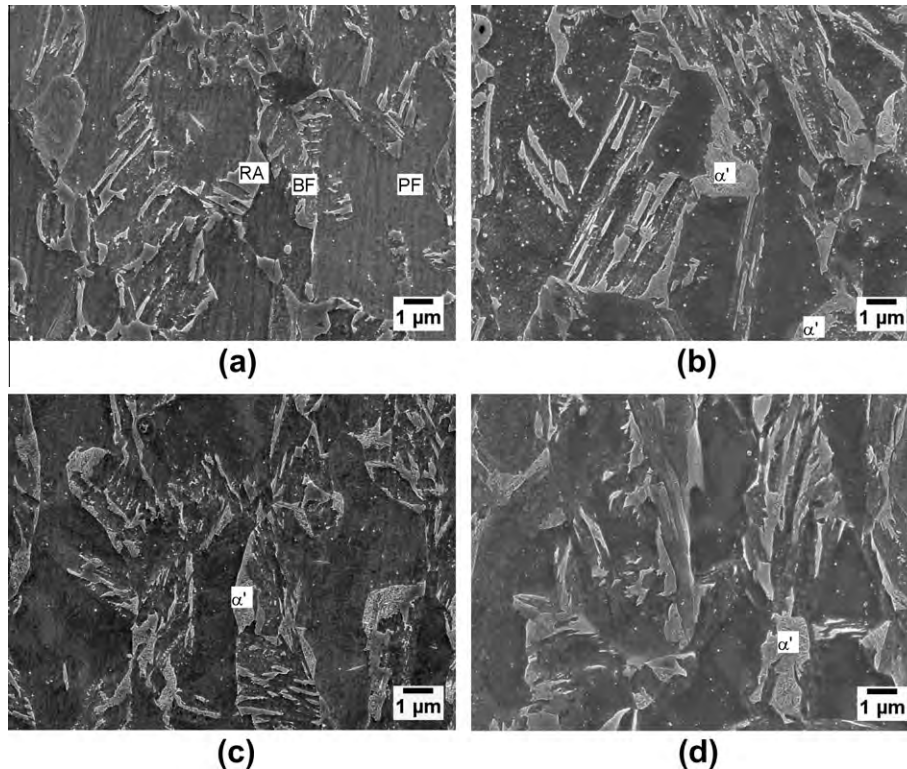

Fig. 1. SEM images of nondeformed microstructure (a) and those fractured (away from necking) in tensile tests at −20 °C (b), 20 °C (c) and 40 °C (d).
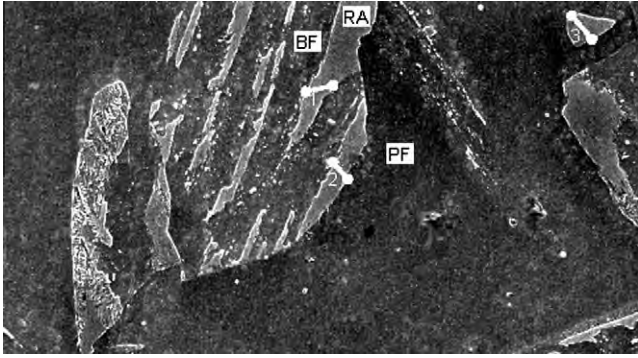
Fig. 2. Schematic of categorical chords of RA in TRIP steel. Chord #1 has both ends neighboring BF; chord #2 has one end neighboring BF and the other neighboring PF; chord #3 has both ends neighboring PF.

Table 2
Definitions of (super-) categories of RA chords.

Super-category	Definition
All	All RA
Adjacent to BF	At least one chord end on the BF/RA interface
Inside BF	Both chord ends on the BF/RA interface
Adjacent to PF	At least one chord end on the PF/RA interface
Inside PF	Both chord ends on the BF/RA interface

4. Results

4.1. Effect of temperature on tensile properties

Fig. 3a shows the engineering stress–engineering strain curves obtained at three testing temperatures and Table 3 summarizes the results. Total and uniform elongations increase when the testing temperature increases from −20 °C to 20 °C, while little change in elongation occurs when the testing temperature increases further to 40 °C. The ultimate tensile strength decreases when the testing temperature increases from −20 °C to 20 °C; further increasing the temperature to 40 °C does not substantially affect the tensile strength. The temperature dependence of

the tensile tests is largely attributed to the temperature dependence of TRIP effect, or specifically the stability of RA.

The instantaneous strain hardening index, n, which indicates how fast a material hardens with strain, also shows a strong variation with temperature between −20 °C to 20 °C, as shown in Fig. 3b. The value of n is calculated by

$$n = \frac{d \ln \sigma}{d \ln \varepsilon} \tag{6}$$

where σ is true stress and ε is true strain in a tensile test. Fig. 3b shows that the value of n as a function of strain is very similar for both the 20 °C and 40 °C tests: in both, after yielding, the strain hardening index slowly increases with increasing strain. The test performed at −20 °C, on the other hand, exhibits a different dependence of n on strain. Overall, n at −20 °C is higher than at 20 °C and at 40 °C up to approximately 0.2 strain. Furthermore, n increases more rapidly with strain after yielding at −20 °C until it reaches a peak value, then decreases until failure. The difference in behavior between the three temperatures is attributed to RA having less stability at −20 °C, which results in significant strain hardening at lower strains compared to the specimens tested at the higher temperatures, where austenite transformation occurs more gradually with strain.

4.2. Effects of testing temperature on RA stability and grain size

The effects of test temperature on stability are shown by the evolution of the RA volume fractions with strain. The total volume fraction of RA is calculated from Eq. (5) based on CCLD measurements. Fig. 4 shows that RA is less stable at −20 °C whereas there is no significant difference between 20 °C and 40 °C. CCLD measurements make it possible to study the effect of temperature on RA with different neighboring microconstituents. Fig. 5 shows the evolution of RA under four categories defined by neighboring microconstituents. RA inside/adjacent to PF undergoes
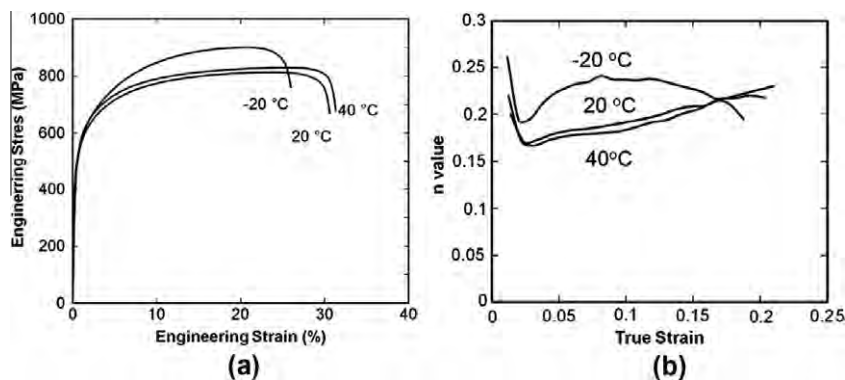

Fig. 3. Uniaxial tensile tests performed at different temperatures: (a) engineering stress–engineering strain curves; (b) instantaneous strain hardening index.

Table 3
Results of tensile tests performed at −20 °C, 20 °C, and 40 °C.

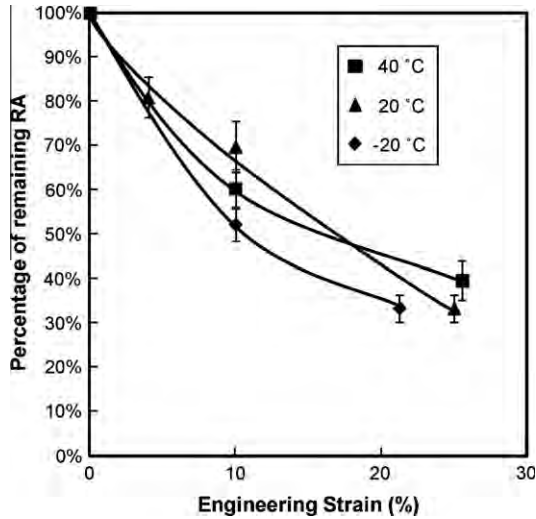| Temperature (°C)	Yield strength (MPa)	Tensile strength (MPa)	Uniform elongation (%)	Total elongation (%)
−20	264	901	20.6	26.0
20	360	813	24.0	30.6
40	309	829	24.8	31.3

Fig. 4. Evolution of total volume fractions of RA with tensile strain. Error bars represent 95% confidence intervals.

SIMT more rapidly as the temperature decreases from 40 °C to −20 °C. By contrast, SIMT of RA inside/adjacent to BF does not show a clear trend with temperature.

Fig. 6 shows the evolution of RA size with engineering tensile strain at the three test temperatures. The average size of RA decreases with strain near PF, but there is no significant change in RA size near BF. Although the test temperature has some influence on the evolution of RA volume fraction, it does not appear to have a strong effect on the evolution of RA size with strain. The average size of RA inside PF decreases slightly faster at the lowest testing temperature.

5. Discussion

The evolution of RA volume fraction, grain size and grain size distribution with plastic strain, measured with the CCLD, can be used to characterize the effects of neighboring microconstituents and RA grain size on its stability. The analysis of the effect of neighboring microconstituents is accomplished by directly comparing transformation kinetics across various categories of chords. The analysis of the effect of RA grain size is complicated by RA islands, which only partly transform to martensite at a given plastic strain. Thus, CCLD values ($n^{ij}(l)$), specifically for RA adja-

cent to martensite, may either increase or decrease with plastic strain, which makes it difficult to mathematically model the evolution of the CCLD with strain. A cumulative function was formulated so that it monotonically decreases with plastic strain and therefore becomes easier to model:

$$P_\varepsilon^{ij}(L) = \int_L^\infty n_\varepsilon^{ij}(l) l \, dl \tag{7}$$

where $n_\varepsilon^{ij}(l)$ is the CCLD at plastic strain ε, and $P_\varepsilon^{ij}(L)$ is the total length of RA chords longer than L in the category ij and at plastic strain ε per unit area of a micrograph. By definition, $P_\varepsilon^{ij}(L)$ is a decreasing function of L and the maximum is reached at $L = 0$, where $P_\varepsilon^{ij}(0)$ is the total length of chords in the category ij at plastic strain ε. The volume fraction of RA as a function of neighboring microconstituents (ij) and RA size can be calculated from $P_\varepsilon^{ij}(L)$:

$$V_\varepsilon^{ij}(l) = V_\varepsilon \frac{P_\varepsilon^{ij}(l)}{\sum_{ij} P_\varepsilon^{ij}(0)} \tag{8}$$

where $V_\varepsilon^{ij}(l)$ is the volume fraction of RA with chord length longer than l in the category ij; V_ε is the total volume fraction of RA at plastic strain ε. V_ε^{ij} is defined as the volume fraction of RA in category ij. The stability of RA adjacent to each microconstituent can be compared with the values of $V_\varepsilon^{ij}(0)$ for each category. The evolution of $V_\varepsilon^{ij}(l)$ with plastic strain depends on both neighboring microconstituents (ij) and RA size (l). In an attempt to quantify these effects, a model for SIMT was developed based on the Burke–Matsumura–Tsuchida (BMT) model. The BMT model is a phenomenological equation for martensitic transformation under plastic strain [16–18]:

$$\frac{V_0 - V_\varepsilon}{V_\varepsilon} = \frac{k}{p} \varepsilon^p \tag{9}$$

where V_0 and V_ε are the volume fractions of RA in undeformed steel and at plastic strain ε, respectively; k is a constant related to the mechanical stability of RA; p is related to the autocatalytic effect and equals 1 for TRIP steels tested at temperatures lower than 60 °C. The constant k, determined by fitting lines to the volume fractions of RA vs. plastic strain data from uniaxial tensile tests, has been used to compare the stability of RA in different TRIP microstructures and under different testing temperatures [7]. The BMT equation was modified to model the size- and microstructure-dependent transformation of RA characterized by the CCLD:

$$\frac{V_0^{ij}(l) - V_\varepsilon^{ij}(l)}{V_\varepsilon^{ij}(l)} = k_1 \exp\left(\frac{l}{L_C}\right) \varepsilon \tag{10}$$

The size- and microstructure-dependent volume fraction $V_\varepsilon^{ij}(l)$ replaces V_ε in Eq. (9). The expression $k_1 \exp(l/L_C)$, which separates the effects of grain size of RA ($\exp(l/L_C)$) and other factors (k_1), replaces the k constant in Eq. (9). By fitting the measured CCLD to Eq. (10), the constants k_1 and L_C are determined and used to describe the
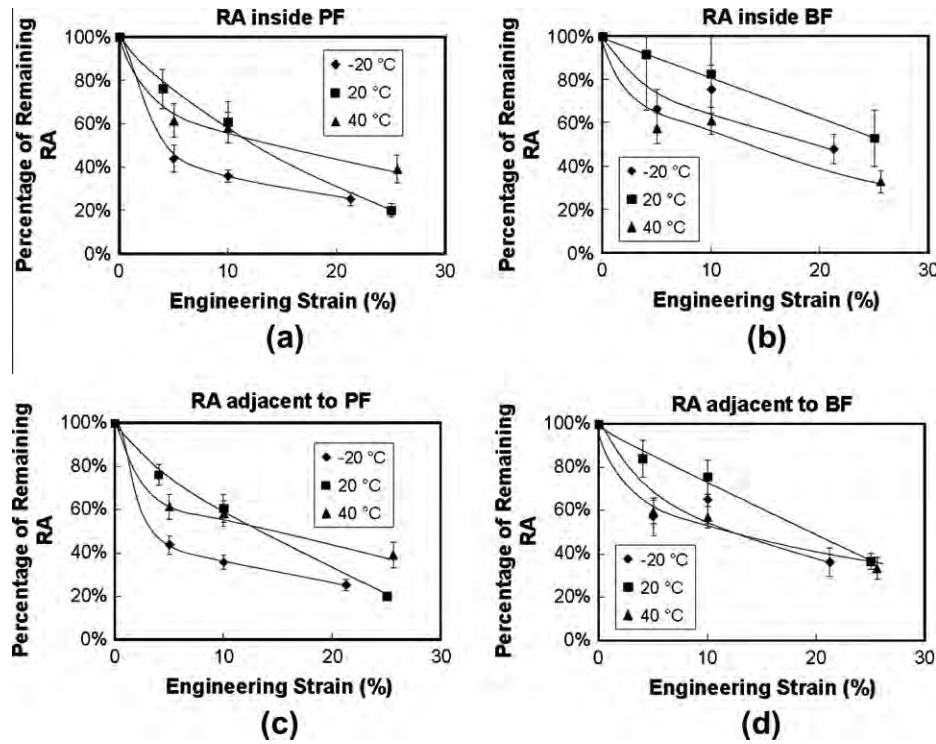
Fig. 5. Effect of temperature on the stability of RA inside PF (a), inside BF (b), adjacent to PF (c) and adjacent to BF (d). Error bars are 95% confidence intervals, calculated by the nonlinear curve fitting function of Matlab.
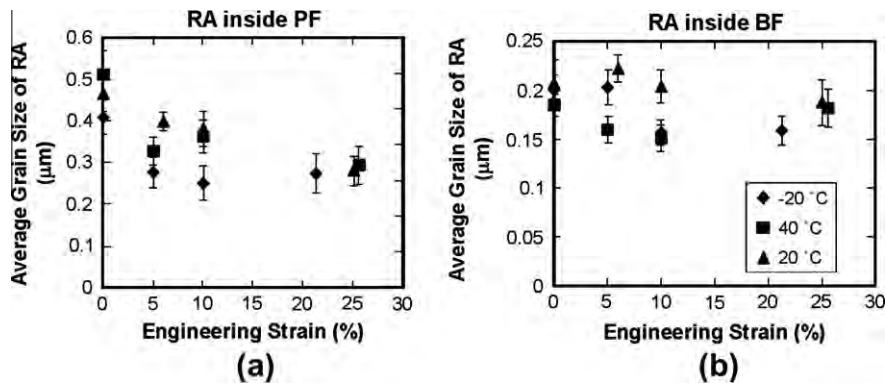

Fig. 6. Average grain sizes of RA inside PF (a) and inside BF (b). Error bars represent 95% confidence intervals.

size-dependent SIMT kinetics of RA with specified neighboring microconstituents. The aforementioned statistical-kinetics modeling approach was applied to CCLD measurements of the TRIP steel microstructures at multiple tensile strain levels as "snapshots" of the evolving microstructures during a tensile test. The CCLD data was first converted to size-dependent RA volume fractions using Eqs. (7) and (8) and then fitted to Eq. (10) using the non-linear curve fitting function of MatLab.

Fig. 7a shows the model parameter L_C of RA with different neighboring microconstituents for the 20 °C tensile tests. Except for RA inside PF, the L_C parameter is statistically similar for the RA categories, indicating a similar RA grain size distribution as well as similar sensitivity of transformation kinetics to RA grain size. The larger L_C

value for RA inside PF might be partially due to the larger grain size of RA inside PF; the average grain size of RA inside PF is 0.44 μm, which is 37% larger than overall average RA grain size (0.32 μm) and 111% larger than the average grain size of RA inside BF (0.21 μm). However, the average grain size of RA adjacent to PF is almost identical to that of RA inside PF, yet the L_C value of the former type of RA is significantly lower than the latter and statistically similar to all other types of RA. Therefore, L_C appears to be only weakly affected by the initial RA grain size. The difference between the L_C of RA inside PF and all other types of RA can be attributed to the difference in the sensitivity of RA stability to RA grain size. As a larger L_C corresponds to less dependence on grain size (Eq. (10)), the transformation kinetics are less sensitive to RA
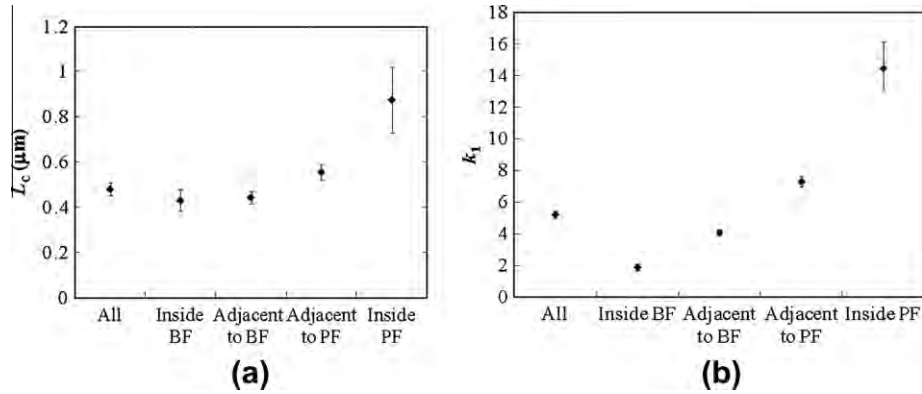
Fig. 7. (a) k_1 and (b) L_C of the modified BMK model in the laboratory heat-treated TRIP steel tested at 20 °C. Error bars are 95% confidence intervals, calculated by the nonlinear curve fitting function of Matlab.
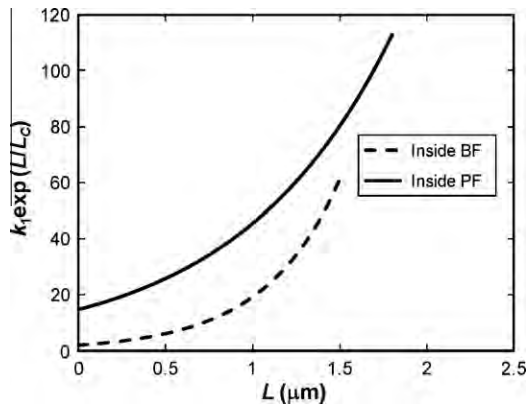

Fig. 8. Plot of $k_1\exp(l/L_C)$ for samples tested at 20 °C. The maximum of L is chosen to represent the lengths of 99% of the chords in each category.

grain size in PF compared to RA with other neighboring microconstituents.

Fig. 7b shows the parameter k_1 at 20 °C. The k_1 value is significantly higher for RA inside PF than RA inside BF. As k_1 is related to the stability of RA (Eq. (8)), the difference in k_1 shows that RA inside PF is less stable than RA inside BF. In addition, the stability of RA, as quantified by k_1, generally increases in the order of RA inside BF, adjacent to BF, adjacent to PF and inside PF. The parameter k_1 by itself quantifies the average stability of RA regardless of size; $k_1\exp(l/L_C)$, on the other hand, quantifies the stability of RA larger than l, as plotted in Fig. 8. The plot shows that RA inside BF is more stable (lower $k_1\exp(l/L_C)$) than RA inside PF for all sizes of RA present in the microstructure, which indicates that the stabilizing effect of BF on RA is not solely attributed to the finer grain size of film RA between BF laths. The stabilizing effect of BF may be explained by two possible mechanisms: local carbon partitioning and stress shielding. The local carbon partitioning mechanism will be discussed first. When BF forms after intercritical annealing and cooling to the bainitic start temperature, it rejects carbon into the adjacent, untransformed RA. As Eq. (1) shows, increasing

carbon content reduces the martensitic transformation driving force, therefore stabilizing RA against thermal- and stress/strain-induced transformation. The stress shielding mechanism is based on the assumption that BF is significantly harder than PF such that RA experiences less stress in a RA–BF composite microstructure than in a RA–PF composite microstructure [4,12]. The significance of each mechanism can be evaluated by exploiting the difference in temperature dependence of the two mechanisms. As shown in Eq. (2), the driving force for transformation decreases proportionally with increasing testing temperature. The stress shielding mechanism, on the other hand, depends on the flow stress of the microconstituents, which does not change substantially within a moderate temperature range around room temperature (e.g. −20 °C to 40 °C).

Steels deformed in temperature-controlled tensile tests were analyzed using CCLD and the size-dependent BMK model. As shown in Fig. 9a and b, L_C does not vary greatly with testing temperature, which is consistent with the observation that the evolution of average RA grain size does not depend on temperature, as shown in Fig. 6. Therefore, it is reasonable to conclude that the RA grain size as a stabilization mechanism does not account for the difference in temperature dependence of transformation kinetics between RA inside PF and BF.

The stability of RA in tensile tests is quantified by the k_1 parameter in the size-dependent BMK model. Fig. 10 shows a plot of the k_1 parameter of different types of RA at different testing temperatures. The value of k_1 for all RA decreases as the temperature increases from −20 °C to 20 °C. The increase in k_1 from 20 °C to 40 °C is unexpected, and is most likely due to errors in curve fitting, as Fig. 5 shows that the transformation kinetics of the TRIP steel tested at 20 °C and 40 °C are comparable. Fig. 10 also shows that the k_1 of RA inside PF decreases rapidly with temperature. In contrast, the k_1 of RA inside BF shows a slight increase as temperature increases ($k_1 = 4.1$ at −20 °C to $k_1 = 7.1$ at 40 °C), which is a weak trend compared to the k_1 of RA inside PF ($k_1 = 44.0$ at −20 °C to $k_1 = 7.6$ at 40 °C). The temperature dependence of k_1
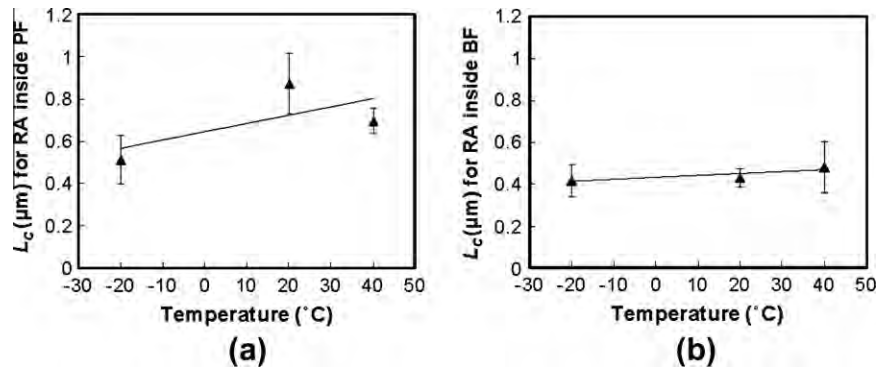
Fig. 9. L_C values of RA inside (a) PF and (b) BF at −20 °C, 20 °C and 40 °C. Error bars are 95% confidence intervals, calculated by the nonlinear curve fitting function of Matlab.
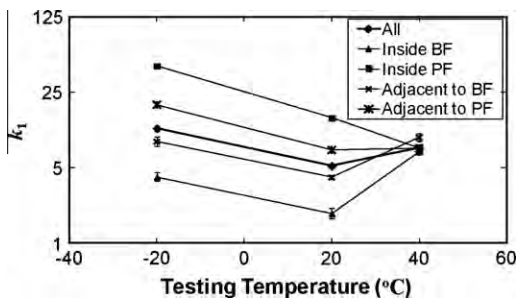

Fig. 10. Plot of k_1 in the size-dependent BMT model for various temperatures and types of RA. Error bars are 95% confidence intervals, calculated by the nonlinear curve fitting function of Matlab.

might be related to changes in the martensitic transformation driving force with temperature. Eq. (2) shows that the driving force of the martensitic transformation increases as temperature decreases; more importantly, the transformation rate decreases with increasing carbon content. In other words, the stability of RA becomes less sensitive to temperature as the carbon content increases. A higher carbon content of RA inside BF, which can be explained by the local carbon partitioning mechanism, could therefore explain its lower temperature sensitivity compared to RA adjacent to PF.

The potential effects of stress shielding related to RA stability were explored with a nanoindentation study of PF and BF in the TRIP steel. A Hysitron TI-950 Nanoindenter was used to perform indentation on PF and BF areas in the microstructure. The topographic imaging capability of the equipment makes it possible to indent on the microconstituent of interest, as shown in Fig. 11. A Berkovich tip with a load of 200 μN was used for the indentation. Indentation was performed on an undeformed sample, and on samples deformed to 4% and 25% plastic strain at room temperature. Hardness was calculated based on the unloading portion of the load–displacement curve. Fig. 12 shows the hardness values of BF and PF. In undeformed samples, BF is significantly harder than PF, which is consistent with Furnémont et al.'s [11] nanohardness measurement results in a TRIP steel. As plastic strain
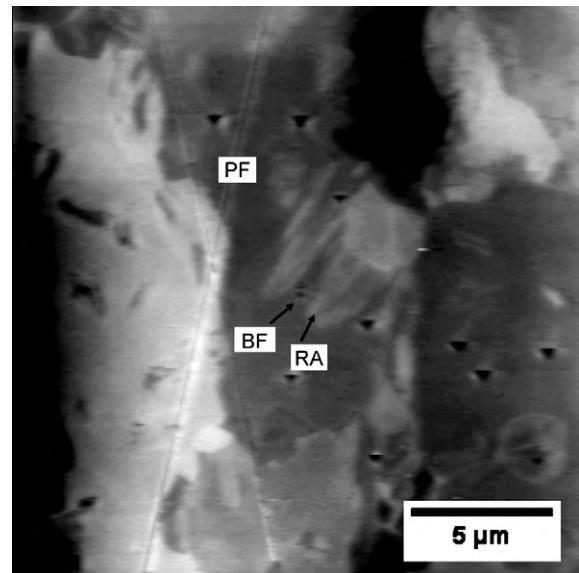

Fig. 11. Topographic image of laboratory heat-treated TRIP steel. Dark triangles are the nanoindents.
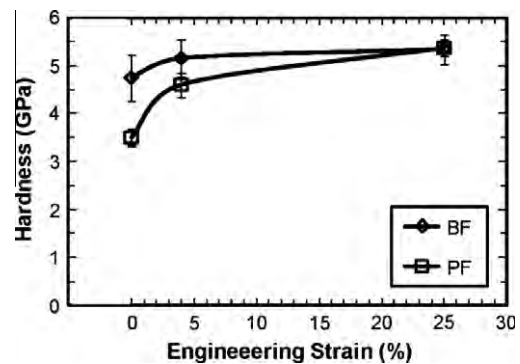

Fig. 12. Hardness of BF and PF in TRIP steels deformed in tensile tests at room temperature. Error bars are 95% confidence intervals.

increases, the hardness of both BF and PF increases due to strain hardening. However, BF hardens significantly slower than PF. The Wilcoxon rank test was used evaluate the significance of the difference in hardness between BF

and PF. At 4% plastic strain, $0.05 < p < 0.01$, indicating a slight difference in hardness; at 25% plastic strain, $p > 0.05$, indicating no statistical difference in hardness between BF and PF. Fig. 5 shows that, at 4% plastic strain, RA inside BF transforms at a lower rate than RA inside PF even though the hardnesses of PF and BF are nearly the same. Therefore, ignoring the morphological differences between the two microconstituents, stress partitioning at that strain level and beyond may not be substantially different in PF and BF, which is consistent with the previously drawn conclusion that local carbon partitioning has a more significant role in stabilizing RA.

6. Summary and conclusions

Interrupted tensile tests have been performed at various controlled temperatures on a multiphase TRIP steel. Microstructures of the steels deformed to various strain levels were characterized using CCLD, a novel technique that simultaneously captures volume fraction, size and neighboring microconstituents of RA. CCLD measurements show that: (i) the average RA grain size decreases with increasing strain; and (ii) RA inside or adjacent to BF is more stable than RA inside or adjacent to PF.

The effects of RA grain size and neighboring microconstituents on RA stability were investigated with a size-dependent BMT model. The model was used to separate the effects of RA grain size and other factors. It is found that BF has a stabilizing effect on neighboring RA, which cannot be attributed solely to finer RA inside/adjacent to BF.

The stabilizing mechanism of BF is studied further by comparing the kinetics of SIMT at three temperatures (-20 °C, 20 °C and 40 °C). Size-dependent BMT modeling reveals that the stability of RA inside PF is significantly more sensitive to temperature than that of RA inside BF, while the effect of RA grain size is largely invariant within the range of temperature. The local carbon partitioning mechanism predicts that RA close to BF is more enriched in carbon, which reduces the temperature sensitivity of transformation driving force (Eq. (2)). Therefore, the observed difference in temperature sensitivity supports the local carbon partitioning mechanism.

The relevance of an alternative stabilizing mechanism, the stress partitioning mechanism, was further evaluated by comparing the nanohardnesses of BF and PF. In this study, nanohardness tests were performed on tensile-tested as well as undeformed TRIP samples. The difference in nanohardness values between the two microconstituents decreases with plastic strain. The difference becomes marginal at 4% plastic strain. Therefore, the stress shielding mechanism might be a minor component of the stabilizing effect of BF.

Both tensile tests and nanohardness tests point to the conclusion that the BF stabilization of RA is caused by local carbon partitioning. This finding may lead to better understanding of how steel composition and process parameters such as bainite transformation temperature and holding times affect RA stability.

Acknowledgements

References

[1] Haidemenopoulos GN, Vasilakos AN. J Alloy Compd 1997;247:128.
[2] Brandt ML, Olson GB. Ironmaking Steelmaking 1993;20:55.
[3] Timokhina IB, Hodgson PD, Pereloma EV. Metallurgical and materials transactions a – physical metallurgy and. Metall Mater Trans A – Phys Metall Mater Sci 2004;35:2331.
[4] Jacques PJ, Ladriere J, Delannay F. Metall Mater Trans A 2001;32:2759.
[5] Haidemenopoulos GN, Vasilakos AN. Anglais 1996;67:513.
[6] Jiménez JA, Carsí M, Ruano OA, Frommeyer G. Mater Sci Eng A 2009;508:195.
[7] Samek L, De Moor E, Penning J, De Cooman B. Metall Mater Trans A 2006;37:109.
[8] Islam MA, Chen S, Tomota Y. J Mater Eng Perform 2007;16:248.
[9] Sugimoto KI, Misu M, Kobayashi M, Shirasawa H. ISIJ Int 1993;33:8.
[10] Grajcar A. J Achieve Mater Manuf Eng Acta Mater 2010;39:7.
[11] Furnémont Q, Kempf M, Jacques PJ, Göken M, Delannay F. Mater Sci Eng A 2002;328:26.
[12] Gao G, Hutchinson JW, McMeeking RM. Mech Mater 1991;12:85.
[13] Ros-Yanez T, Houbaert Y, Mertens A. Mater Charact 2001;47:93.
[14] Zhang S, Findley K. Metallogr Microstruct Anal 2012;1:28.
[15] Li M, Wilkinson D. Chem Eng Sci 2005;60:3251.
[16] Burke J. Kinetics of phase transformations in metals. Oxford: Pergamon Press; 1965.
[17] Matsumura O, Sakuma Y, Takechi H. Scr Metall 1987;21:1301.
[18] Tsuchida N, Tomota Y. Mater Sci Eng A 2000;285:346.